Progress in Biophysics and Molecular Biology 105 (2011) 67–79

Contents lists available at ScienceDirect

Progress in Biophysics and Molecular Biology

journal homepage: www.elsevier.com/locate/pbiomolbio

Original Research

Exploiting the potential of three dimensional spatial wavelet analysis to explore nesting of temporal oscillations and spatial variance in simultaneous EEG-fMRI data

Matthias Schultze-Kraft [a,b,*], Robert Becker [a,b], Michael Breakspear [e,f], Petra Ritter [a,b,c,d,*]

[a] Bernstein Focus State Dependencies of Learning & Bernstein Center for Computational Neuroscience Berlin, Charitéplatz 1, 10117 Berlin, Germany
[b] Department of Neurology, Charité – University Medicine Berlin, Campus Charité Mitte, 10117 Berlin, Germany
[c] Max Planck Institute for Human Cognitive and Brain Sciences, Stephanstr. 1, 04303 Leipzig, Germany
[d] Berlin School of Mind and Brain & Mind and Brain Institute, Humboldt University Berlin, Luisenstr. 56, 10117 Berlin, Germany
[e] Queensland Institute of Medical Research and the Royal Brisbane and Woman's Hospital, Brisbane, Queensland 4006, Australia
[f] School of Psychiatry, University of New South Wales and The Black Dog Institute, Sydney, New South Wales 2031, Australia

ARTICLE INFO

Article history:
Available online 19 November 2010

Keywords:
Three dimensional spatial wavelet analysis
EEG-fMRI
Alpha rhythm
Synchrony
Spatiotemporal nesting

ABSTRACT

Synchronization of the activity in neural networks is a fundamental mechanism of brain function, putatively serving the integration of computations on multiple spatial and temporal scales. Time scales are thought to be nested within distinct spatial scales, so that whereas fast oscillations may integrate local networks, slow oscillations might integrate computations across distributed brain areas. We here describe a newly developed approach that provides potential for the further substantiation of this hypothesis in future studies. We demonstrate the feasibility and important caveats of a novel wavelet-based means of relating time series of three-dimensional spatial variance (energy) of fMRI data to time series of temporal variance of EEG. The spatial variance of fMRI data was determined by employing the three-dimensional dual-tree complex wavelet transform. The temporal variance of EEG data was estimated by using traditional continuous complex wavelets. We tested our algorithm on artificial signals with known signal-to-noise ratios and on empirical resting state EEG-fMRI data obtained from four healthy human subjects. By employing the human posterior alpha rhythm as an exemplar, we demonstrated face validity of the approach. We believe that the proposed method can serve as a suitable tool for future research on the spatiotemporal properties of brain dynamics, hence moving beyond analyses based exclusively in one domain or the other.

1. Introduction

There is evidence that the synchronization of neural networks enables the brain to functionally integrate computations on multiple spatial and temporal scales (Buzsáki et al., 2003; Bushara et al., 2003). Oscillations in the higher frequency range are thought to facilitate communication between local brain areas, whereas lower frequency oscillations are thought to be associated with wide range communications (Buzsáki, 2006). This approach suggests an intriguing notion that time scales are not only nested within one another (Jensen and Colgin, 2007) but also within distinct spatial scales. The aim of this study is to describe a new technique, which provides the potential to further substantiate this hypothesis. This approach basically constitutes a new way of analysis of simultaneously recorded electroencephalography (EEG-) and functional magnetic resonance imaging (fMRI) (Ritter and Villringer, 2006) data. The main idea is to utilize complementary information provided by the two methods, which is high spatial resolution in the case of fMRI and high temporal resolution in the case of EEG, to investigate a possible nesting of temporal oscillations within distinct spatial scales of brain activity. We hence explore for the first time the feasibility of relating time series of three-dimensional spatial variance (energy) of fMRI data to time series of temporal variance of EEG data through appropriate wavelet decompositions in both domains. In other words, we evaluate the potential of 3D spatial wavelet analysis of fMRI data for the investigation of the hypothesized link between the spatial extent of active neuronal

* Corresponding authors at: Department of Neurology, Charité, University Medicine Berlin, Charitéplatz 1, 10117 Berlin. Tel.: +49 30 450560005; fax: +49 30 450560936.
E-mail addresses: matthias.schultze-kraft@bccn-berlin.de (M. Schultze-Kraft), petra.ritter@charite.de (P. Ritter).

0079-6107/$ – see front matter © 2010 Elsevier Ltd. All rights reserved.
doi:10.1016/j.pbiomolbio.2010.11.003

populations and varying EEG rhythms. Our approach is based on the fact that local signal changes (such as local changes in fMRI activity) are reflected by high energy at fine spatial scales while more distributed sources of signal changes (such as larger clusters of fMRI activity) are expected to be associated with higher energy at coarser spatial scales in 3D wavelet decompositions.

The application of wavelets to fMRI data analysis is fairly young, given that the widespread use of wavelets for signal processing actually started almost 20 years ago with the work of Daubechies (1992). Among the first to employ wavelets for fMRI data analysis were Ruttiman and coworkers (1995). In their study, the problem of high intervoxel correlations in the spatial domain was addressed. They decorrelated – or pre-whitened – single slices of blood oxygenation level dependent (BOLD) fMRI images by exploiting the decorrelating property of the wavelet transform with two dimensional spatial wavelets. Using this approach, the adjustment factor for multiple testing decreased, which resulted in lower detection thresholds and increased sensitivity of the method to true underlying effects. Similarly, Hilton and coworkers (Hilton et al., 1996) devised a method for increasing the SNR in fMRI data. For this purpose, they decomposed single slices of BOLD images into several spatial scales and applied a nonlinear soft-thresholding operation to each wavelet coefficient at the finer scales, thereby essentially smoothing the data. Brammer (1998) refined this idea by extending the wavelet transform into three dimensions. Slice-wise wavelet decomposition was performed with two spatial dimensions and time as third dimension, followed by a spatial smoothing in the wavelet domain and a temporal wavelet denoising. Other studies, such as Bullmore et al. (2001), Fadili and Bullmore (2002) and Breakspear et al. (2004), have suggested the use of resampling schemes to accurately ascertain null distributions of activation statistics. To this end, the time courses of fMRI data were wavelet decomposed and a least-squares likelihood function was optimized in the wavelet domain. In a similar manner, several recent studies have extended and improved the utilization of the decorrelating property of the wavelet transform, for instance by explicitly modelling autoregressive components in the fMRI data (Long et al., 2004), integrating wavelet-based spatial decompositions for statistical inference (Van De Ville et al., 2004) or even performing a 4D analysis along all three spatial and the temporal dimension (Dinov et al., 2005).

Suggesting spatial wavelet analysis as a potential tool to examine the multiscale structure of the dynamics of spatial BOLD variance, Breakspear and colleagues (2006) analyzed wavelet-decomposed fMR images associated with evoked cortical activity. To this end they first identified the location of voxels showing the strongest response to visual stimuli. After 2D wavelet decomposition of each image slice, they analyzed the correlation structure of the temporal dynamics of wavelet coefficients associated with the voxels of evoked activity across different scales. This analysis revealed strong correlations within and between different spatial scales, suggesting an inherent multiscale property of cortical activity. The authors argued that these findings support the hypothesis that neural responses have specific multiscale functional connectivities.

The studies mentioned in the penultimate paragraph all have one thing in common: The wavelet transform is basically used as an instrument for smoothing, denoising or decorrelation of neuroimaging data with the eventual purpose of improving the results of subsequent statistical significance tests or explicitly yielding significances. For this purpose, the application of wavelets has already proven to be a valuable and powerful option. However, the full potential of this method may not have been fully exploited. As the results from the study of Breakspear and colleagues show, an explicit analysis of wavelet-coefficient time courses provides an improved understanding of the multiscale properties of large-scale brain activity. This applies especially in the case of simultaneous EEG-fMRI, where the well-known oscillatory bands are examined by decomposing the EEG into frequency-specific temporal dynamics. In order to test the hypothesis of specific relations between temporal and spatial dynamics of brain activity, it seems intuitive to apply the same scale-specific decomposition to the simultaneously acquired BOLD signal.

3D wavelet analyses of fMRI data bears the potential to reveal such systematic relations between the spatial distribution of neuronal activity and temporal dynamics of neuronal rhythms. At the same time it offers the possibility of localization, i.e. pinpointing identified links between spatial and temporal scales to specific brain regions. These properties may be beneficial for the understanding of the functional roles of neuronal rhythms visible in EEG.

Prominent EEG rhythms show up in characteristic frequency bands and are assumed to result from synchronized postsynaptic activity of a large number of neurons. The most prominent human EEG rhythm is the posterior alpha rhythm, which was discovered with the advent of EEG in 1929 by Berger (1929). This rhythm has its peak energy in the 8–12 Hz range and is a robust phenomenon that can typically be observed in posterior scalp areas in alert relaxed subjects when they have their eyes closed.

Previous combined EEG-fMRI studies have demonstrated negative correlations between slow power or amplitude fluctuations of the posterior alpha rhythm and the cortical fMRI signal in specific – mostly occipital – regions (Goldman et al., 2002; Moosmann et al., 2003; Laufs et al., 2003; Feige et al., 2005; Goncalves et al., 2005; de Munck et al., 2007; Difrancesco et al., 2008). Similarly, for other EEG frequency bands ranging from delta (1–4 Hz) and theta (4–8 Hz) (Mantini et al., 2007; Ritter et al., 2008a) to beta (Mantini et al., 2007; Laufs et al., 2003; Ritter et al., 2008a, 2009], gamma (30–100 Hz) (Mantini et al., 2007; Ritter et al., 2008a; Mulert et al., 2010) and even ultra-high frequency bands (Ritter et al., 2008b) correlations with the fMRI signal in specific regions have been demonstrated. Also simultaneous EEG and near infrared spectroscopy (NIRS) recordings in humans (Koch et al., 2009) and intracortical recordings in cats (Niessing et al., 2005) revealed correlations between spontaneous power fluctuations in the gamma band and hemodynamics. In most cases hemodynamic correlates of rhythms were found in the structures that were presumed to generate the respective rhythm. Hence two important prerequisites for the here proposed approach are met: EEG rhythms are associated with fMRI signal changes and these changes largely reflect the topographic distribution of putative rhythm-generator networks.

For proof of concept of the present proposed approach, we select the most prominent and best-investigated EEG rhythm in general terms and in terms of combined EEG-fMRI, which is the posterior alpha rhythm.

We demonstrate the feasibility of relating spatial frequencies of fMRI activity to the posterior EEG alpha rhythm and of identifying the major caveats. To this end, we employed the three-dimensional dual-tree complex wavelet transform in order to overcome one of the principle limitations of the traditional three dimensional discrete wavelet transform employed in Breakspear et al. (2006), namely the lack of translational invariance and directional selectivity. We also tested our algorithm on artificial signals with known signal-to-noise ratios and compared these to decompositions of real fMRI data.

In this paper we focus on the face validity and technical aspects of our analysis. In a subsequent paper we will apply the techniques described here to address the hypothesis that the hemodynamic correlates of low (e.g., alpha) frequency neuronal dynamics have energy at larger spatial scales. While, conversely, the hemodynamic

correlates of high (e.g., gamma) activity are expressed predominantly at high spatial scales (frequencies). We do not address this particular hypothesis in this paper; however, we provide an illustrative analysis that focuses on the spatial expression (as measured with fMRI) of low frequency alpha power (as measured with EEG). We will see that the expression of low frequency endogenous activity best predicts fMRI responses over larger spatial scales, relative to small spatial scales.

2. Materials and methods

2.1. Methods overview

In this section we describe our analysis approach, which consists of the following steps

1. EEG power changes in the occipital alpha band were computed via continuous wavelet transform (CWT) and subsequently convolved with the canonical hemodynamic response function, yielding a predicted time course of associated slow frequency neuronal changes.
2. Each preprocessed fMR image was decomposed into three spatial scales by means of a three-dimensional dual-tree complex wavelet transform (3D DT-CWT).
3. Time series of wavelet coefficients were correlated with a temporal predictor variable (e.g. the power changes in 1.), yielding one multiscale spatiotemporal correlation (MSC) map for each spatial scale.
4. A back projection of MSC maps into native space was obtained on the basis of the inverse 3D DT-CWT.

2.2. Experimental setup

A subset of four data sets was used for our analyses, only healthy, adult volunteers (3 females; mean age, 24.75 years) were used. Written informed consent was obtained from each subject before participation. Subjects were requested to rest with eyes closed while maintaining alertness. Acquisition time averaged to 30 min. EEG data were acquired from 29 scalp channels and recorded simultaneously with fMRI in a 1.5 Tesla MR Vision scanner (Siemens Vision) using a T2*-weighted BOLD-sensitive gradient echo planar imaging (EPI) sequence (scan repetition time, 2200 ms; acquisition time, 2050 ms; echo time, 60 ms; volumes, 750; slices, 20; voxel size, $3.3 \times 3.3 \times 5.5$ mm). EEG data acquisition was done using magnetic-resonance compatible amplifiers (BrainAmp; Brain Products) and EEG caps (Easy-Cap; FMS) arranged according to the International 10–20 System, referenced against an electrode at FCz. Impedances of all electrodes were set below 5 kΩ. Subjects were wearing earplugs and the light was turned off.

2.3. EEG data analysis

The four EEG data sets acquired simultaneously with fMRI contained artefacts from MR gradient switching and ballistocardiogram (BCG) effects generated by heart-beat associated blood flow changes and movements of the electrodes in the static field of the MR scanner (Debener et al., 2008). Both classes of artefacts were corrected using template estimation and subtraction (Ritter et al., 2007, 2010), as implemented in the Vision-Analyzer software (version 1.03; Brain Products). Subsequently, the posterior alpha rhythm was semi-automatically identified by means of an independent component analysis (ICA) of all EEG channels. This allowed the spectral dynamics of EEG data from electrode O2 to be determined. After low-pass filtering of the signal at 70 Hz, the data were then decomposed by means of a continuous wavelet transform. For this purpose the component time series was convolved with a Morlet wavelet, where the frequency sensitivity is inversely related to the scaling parameter of the wavelet. By applying wavelet decomposition to the data in the frequency range between 8 and 12 Hz in steps of 0.5 Hz and squaring the resulting wavelet coefficients, the power of the alpha rhythm was determined. Finally, spectral power changes averaged over the 8 to 12 Hz alpha band were convolved with the canonical hemodynamic response function (HRF) (Friston et al., 1995a) and subject to linear detrending using Matlab 7.4 (The Mathworks, Natick, MA).

2.4. fMRI data analysis

2.4.1. Preprocessing

The analysis of fMR images by means of 3D wavelet decomposition differs from traditional approaches (e.g. the general linear model, GLM) in its preprocessing requisites. Raw fMR images show large inhomogeneities regarding acquisition space and time: Typically, in echo planar imaging sequences the single planes, which compose an image are acquired at different times. Furthermore, the size of the voxels is anisotropic, i.e. the voxels are larger along the dimension orthogonal to the planes. And finally, movement of the head during recording frequently results in strong artefacts.

In the 3D spatial wavelet decomposition of BOLD images the spatial wavelets are moved along the image in multiple directions (for details, see Fig. 1), thus requiring the whole image to be instantaneous in time and being defined in an isotropic space. In order to correct for timing differences across slices, a slice timing correction was applied to each fMR image.

An estimate of the spatial displacement of the subject's brain due to movement over time can be calculated by SPM8's realignment routine. This routine uses a least squares approach in order to define the optimal realignment of a series of fMRI scans by determining for each image the six parameters for a rigid body transformation. These parameters consist of shifts (denoted x, y and z) and rotations (pitch, roll, yaw) on the three main axes (Friston et al., 1995b). Before 3D spatial wavelet decomposition, images were corrected by this standard realignment routine.

Despite employment of realignment correction algorithms residual movement-related variance is known to remain in EPI images (Friston et al., 1996) – predominantly at the brain surfaces, i.e. at external (brain-skull) and internal (brain-ventricles) tissue borders, i.e. at sites of field inhomogeneities (Andersson et al., 2001). Using a multiple regression model, the residual variance in the voxel time series explained by the realignment parameters can be estimated. While traditional analyses of fMRI data using a GLM implicitly include this estimate as confounding variables in the linear model, we chose the equivalent approach of explicitly subtracting the estimate from the data before correlation analysis.

Subsequently, a three-dimensional linear interpolation resampling was performed on each image in order to provide images in isotropic space. And finally, a 3D mask was defined that excluded all voxels corresponding to non-brain tissue. The brain mask was determined by the Brain Extraction Tool (FMRIB Software Library, University of Oxford).

2.4.2. Selection of an appropriate wavelet transform for fMRI

The wavelet transform decomposes the total energy or variance of some time series or spatial process associated with a set of wavelet functions, each of which is weighted by a coefficient representing the amount of energy or variance in the data at a specific scale and location. A wavelet function $\psi(x)$ is a finitely extended,

compactly supported wave whose oscillations decay rapidly towards zero and is dilated and translated as

$$\psi_{a,b}(x) = \frac{1}{\sqrt{a}}\psi\left(\frac{x-b}{a}\right), \quad (1)$$

where a and b are the dilation and the translation parameters, respectively. The wavelet decomposition of a real valued function $f(x)$ can be obtained by computing the inner product of the wavelet functions and the data:

$$c_{a,b} = \langle f, \psi_{a,b} \rangle = \int f(x)\psi_{a,b}(x)\,dx, \quad (2)$$

where $c_{a,b}$ are called wavelet coefficients. Two types of the wavelet transform exist. In the continuous wavelet transform (CWT), the dilation and translation parameters a and b define any point on the half plane $\mathbb{R}_+ \times \mathbb{R}$. This property renders the CWT particularly suited for describing the dynamics of spatial or temporal processes in specific frequencies. However, this comes at the expense of severely increasing the required computation time and memory when performing a multiscale analysis of a signal because the decomposition is redundant (i.e. it provides an over-complete tessellation of the time-frequency plane). The discrete wavelet transform (DWT) overcomes this problem by confining the dilation and translation on a discrete subset of the real half plane in the continuous case. Furthermore, by introducing a so called scaling function $\varphi(x)$, it allows for an efficiently computable, compact multi-resolution analysis of the signal (Daubechies, 1988).

The scaling and wavelet functions are not usually computed explicitly but rather the transform is performed using high pass and low pass filters called quadrature mirror filters. One of the most commonly used algorithms for a DWT based multi-resolution analysis is Mallat's decimated dyadic filter tree, also called the pyramidal algorithm (Mallat, 1989; Daubechies, 1990, 1993). The algorithm proceeds iteratively and decomposes the data using a filter bank of wavelets. In successive stages the scalar products of the high-pass and the low-pass filters with the data are computed, the resulting detail and approximation coefficients are then dyadically down-sampled, and the approximation coefficients from the previous stage are taken as the data vector in the next stage. These iterations are continued until the coarsest desired scale coefficients are produced. Obviously, a signal of length 2^J can be decomposed into at most J scales. In this way, a J-scale decomposition of a signal $f(x)$ by means of a discrete wavelet transform can be written as:

$$f(x) = \sum_k a_{J,k}\varphi_{J,k}(x) + \sum_j \sum_k d_{j,k}\psi_{j,k}(x), \quad (3)$$

where $a_{J,k}$ are the approximation coefficients of the last stage and $d_{j,k}$ the detail coefficients of all preceding stages. Provided that a given wavelet is perfectly orthogonal, this decomposition can be reversed yielding a perfect reconstruction of the original data. Therefore, in a similar manner, at each stage the signal is convolved with the time-reversed version of the wavelet filters and then dyadically upsampled. This procedure is referred to as the inverse wavelet transform. The wavelet transform can be extended to higher dimensions in a straightforward way by carrying out one-dimensional wavelet decompositions for each dimension separately (Weeks and Bayoumi, 2003).

The conventional DWT has several disadvantages. One of them is its non-invariant behaviour regarding shifts, which means that small shifts of the input data can result in dramatic changes in the wavelet coefficients. For the objective of analyzing the spatial variance in time series of MR images, this can introduce spurious findings due to shifts in the spatial domain caused by residual subject movement. Another drawback of the standard DWT is its poor directional selectivity, particularly noticeable at high-dimensional transforms. This results in a major disadvantage in the detection of certain geometric signal features, like ridges and edges in 2D or 3D images. An alternative approach to the common DWT is the dual-tree complex wavelet transform (DT-CWT) (Kingsbury, 1998, 1999, 2001). In this method two filter trees are applied to the data in parallel. The key point is that the filters used in each tree are designed in such a way that the filtered signals of one tree can be interpreted as the real part of a complex wavelet transform and the filtered signal of the other tree can be interpreted as the imaginary part. In this way the DT-CWT becomes approximately shift-invariant and, particularly in its two- and three-dimensional version, directionally selective, yielding a much more precise decomposition of high-dimensional data (Selesnick and Li, 2003).

For technical reasons, it transpires that the filters used in the first stage of the dual-tree CWT must differ from the filters in succeeding stages. As first-stage filters we use the orthogonal, near-symmetric filters presented by Abdelnour and Selesnick (2001), as filters for all other stages we use those presented by Kingsbury (1999).

At each scale, the three dimensional DT-CWT measures the variance in the data along 28 different orientations, where each orientation has its real and imaginary part, thus effectively decomposing the data into 56 sets of spatially scaled, translated and oriented wavelets. For illustration, Fig. 1 depicts the 28 wavelets orientations of the real part.

2.5. Correlation analysis in wavelet space

The EPI sequence in the fMRI recording provided images consisting of 20 planes, each composed of a 64×64 matrix of BOLD intensity values. As stated in the previous section, each image was resampled using linear interpolation in order to obtain an isotropic space. Furthermore, since the algorithm implementing the DT-CWT requires all dimensions of the input data to have dyadic length, the resampled image was padded with zeros, resulting in a volume of size $64 \times 64 \times 64$. For technical reasons, the criterion of the applied DT-CWT algorithm that stipulates a perfect reconstruction begins to break down when the number of decomposition scales is too high. In the case of a 3-dimensional transform, in order to ensure perfect reconstruction this number should not exceed the upper limit $J_{\max} = \log_2(L_{\min}) - 3$, where $L_{\min}$ is the length of the smallest dimension in the data. For the present case this means $J_{\max} = 3$ scales. In correspondence to the spatial frequency of their wavelets, these three scales will be referred to as the fine, medium and coarse spatial scales. For each of the 56 orientations, the decomposition of an image yields three 3-dimensional matrices of wavelet coefficients with sizes $32 \times 32 \times 32$, $16 \times 16 \times 16$ and $8 \times 8 \times 8$ voxels for the fine, medium and coarse scale respectively. We denote the resulting wavelet coefficient time series of N decomposed images as $W_{j,k,d}(t)$ with scale j, position k, orientation d and $t = 1 \ldots N$. Fig. 2A shows, for each spatial scale, representative cross-sections of one decomposed image (at $t = 1$ and for one specific wavelet orientation). Given that the voxels have a size of $3 \times 3 \times 3$ mm after linear interpolation, a wavelet coefficient defines the amount of spatial variance across a piece of data of roughly 6, 12 and 24 mm of length, respectively at each scale.

Now let $S(t)$ be some signal sampled simultaneously and with the same rate as the BOLD images – in our case alpha power convolved with HRF and down-sampled or realignment parameters. By computing the correlation coefficient between each time series $W_{j,k,d}(t)$ and the signal $S(t)$ we obtain a map of coefficients $\rho_{j,k,d}$. We refer to this as the multiscale spatiotemporal correlation (MSC) map of the signal $S(t)$. It consists of a set of 3-dimensional matrices (one for each scale and orientation) containing coefficients that specify the correlation of the signal with the dynamics of spatial variance in a particular scale and orientation. Fig. 2B depicts cross-sections of the scale-specific maps which result by

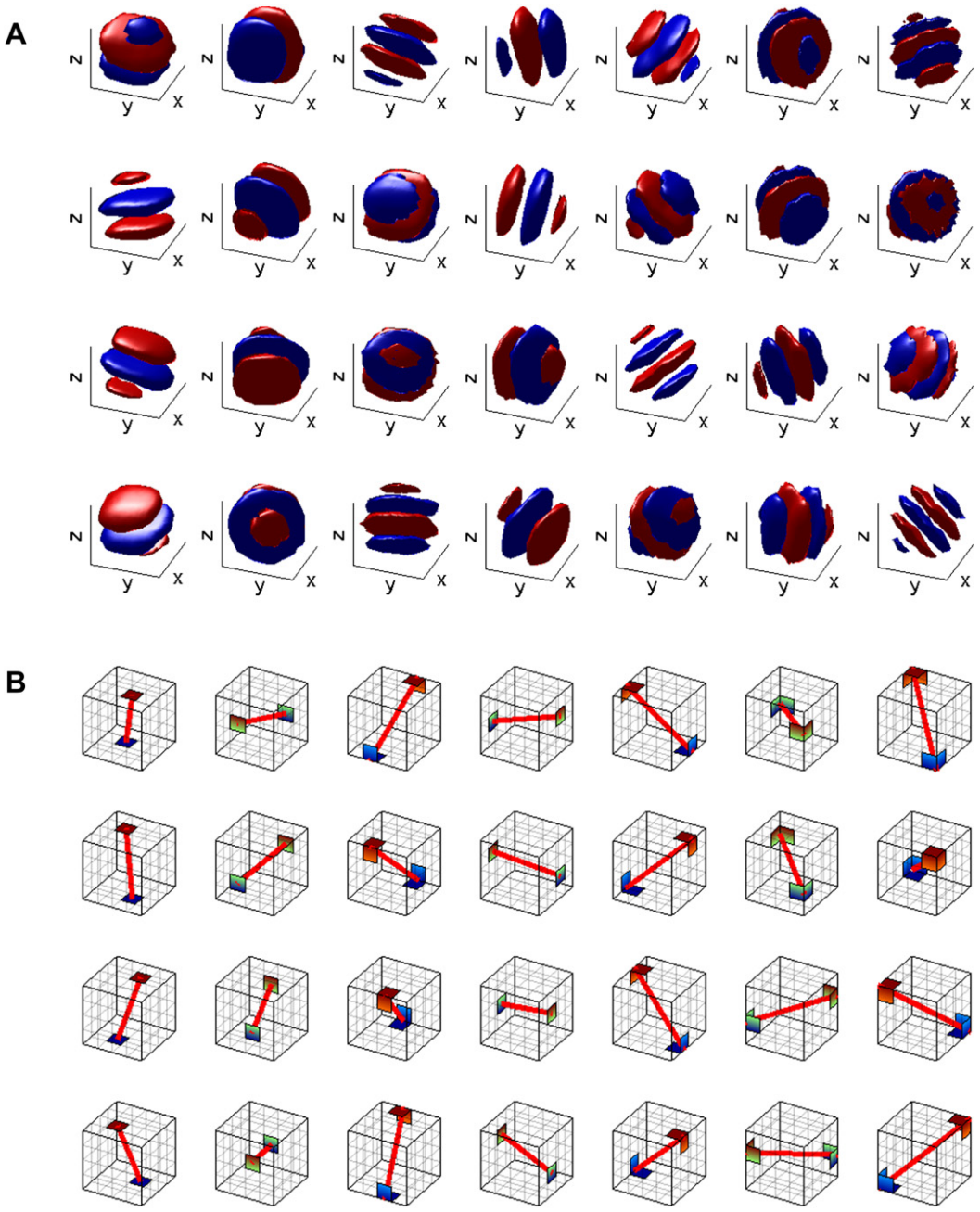

Fig. 1. Orientation selectivity in the 3D dual-tree complex wavelet transform. A: Typical isosurfaces of the real part of the 28 oriented wavelets in the 3-dimensional DT-CWT. Each is generated by reconstructing a unitary wavelet coefficient of a particular orientation and scale, located in the centre of the shown volume. The coloured surfaces correspond to points where the function is equal-valued (red: $\psi_{j,k}(x) = C$, blue: $\psi_{jk}(x) = -C$, C being an arbitrary value). B: The corresponding idealized orientations of the wavelets. In each volume the coloured areas depict the support in the Fourier spectrum of the wavelet in the 3D frequency plane. The connecting red lines are meant to better illustrate their positioning. Wavelets in one column constitute variations of a basic orientation: wavelets in columns 1, 2 and 4 are orientations along the main axes, wavelets in columns 3, 5 and 6 are oriented along the diagonals of two principal axes respectively, whereas wavelets in column 7 represent the four body diagonals of the volume.

correlating the time series of the wavelet coefficient cross-sections shown in 2A with the realignment parameter z-shift.

The correlation coefficients in this map are further tested for their statistical significance using the known distributional characteristics of the correlation coefficients with appropriate degrees of freedom (Bandettini et al., 1993). A threshold of $p \leq 0.05$ was employed. Any non-significant coefficient values were set to zero.

For each subject, two sets of differently preprocessed fMRI data were generated, one with and one without subtraction of residual movement related variance. On each of these two data sets MSC analysis was performed using two types of temporal predictor variables: 1) realignment parameters and 2) EEG alpha band power convolved with HRF. This was done to first demonstrate the impact of residual movement related spatial variance in fMRI data and effects of its proper removal and second to provide face validity of our proposed approach by eventually generating anatomical plausible maps of the scale-specific spatial extent of the alpha rhythm.

2.6. Back projection into native space

Since a multiscale spatiotemporal correlation map lies in wavelet space, a back projection into native space can be achieved

on the basis of an inverse wavelet transform. The use of complex wavelets is particularly useful in this case because the real and the imaginary part of a complex wavelet form a so-called Hilbert transform pair (Selesnick et al., 2005), meaning that they are 90° out of phase with each other. As a consequence, the magnitude of the inverse transform of a complex wavelet does not oscillate around zero but rather provides a smooth positive envelope of the wavelets energy. Hence we denote

$$\eta_j(x) = \sum_d \sum_k \sqrt{\left|\Delta_j \rho_{j,k,d} \psi'_{j,k}(x)\right|^2 + \left|\Delta_j \rho^*_{j,k,d} \psi'_{j,k}(x)\right|^2} \quad (4)$$

as the scale-specific back projection of the multiscale spatiotemporal correlation map ρ, where * denotes the complex conjugate, ψ' is the time reversed version of the wavelet. Furthermore one has to take into account that, due to the dyadic upsampling of the inverse wavelet transform, the energy contained in wavelet coefficients is distributed over extents of data proportional to the scale of the reconstructing wavelet. However, since the coefficients in MSC maps are equally normalized across scales (because they are correlation coefficients), they need to be weighted with the scale-specific factor

$$\Delta_j = \sqrt{2^{D(j-1)}}, \quad (5)$$

where D denotes the dimensionality of the transform ($D = 3$ in our case). That is, in equation (4) at each scale separately, each weighted correlation coefficient $\rho_{j,k,d}$ is inversely transformed both with the real and the imaginary part of the wavelet, whereupon the square root of the sum of their squares is computed. Furthermore, the sum over all wavelet locations k and orientations d is smoothed with a Gaussian kernel of 5 voxels width. We denote such a smoothed sum η_j as the scale-specific back projection of a particular MSC map. The plots in Fig. 2C show the cross-sections of the back projections corresponding to the correlation map cross-sections shown in 2B.

In a final step, a procedure is performed which masks 1) extra-cranial voxels and 2) η-values bellow a certain threshold. We define that threshold value, which we denote θ, by determining a predefined percentile of the distribution of η-values over all scales. For

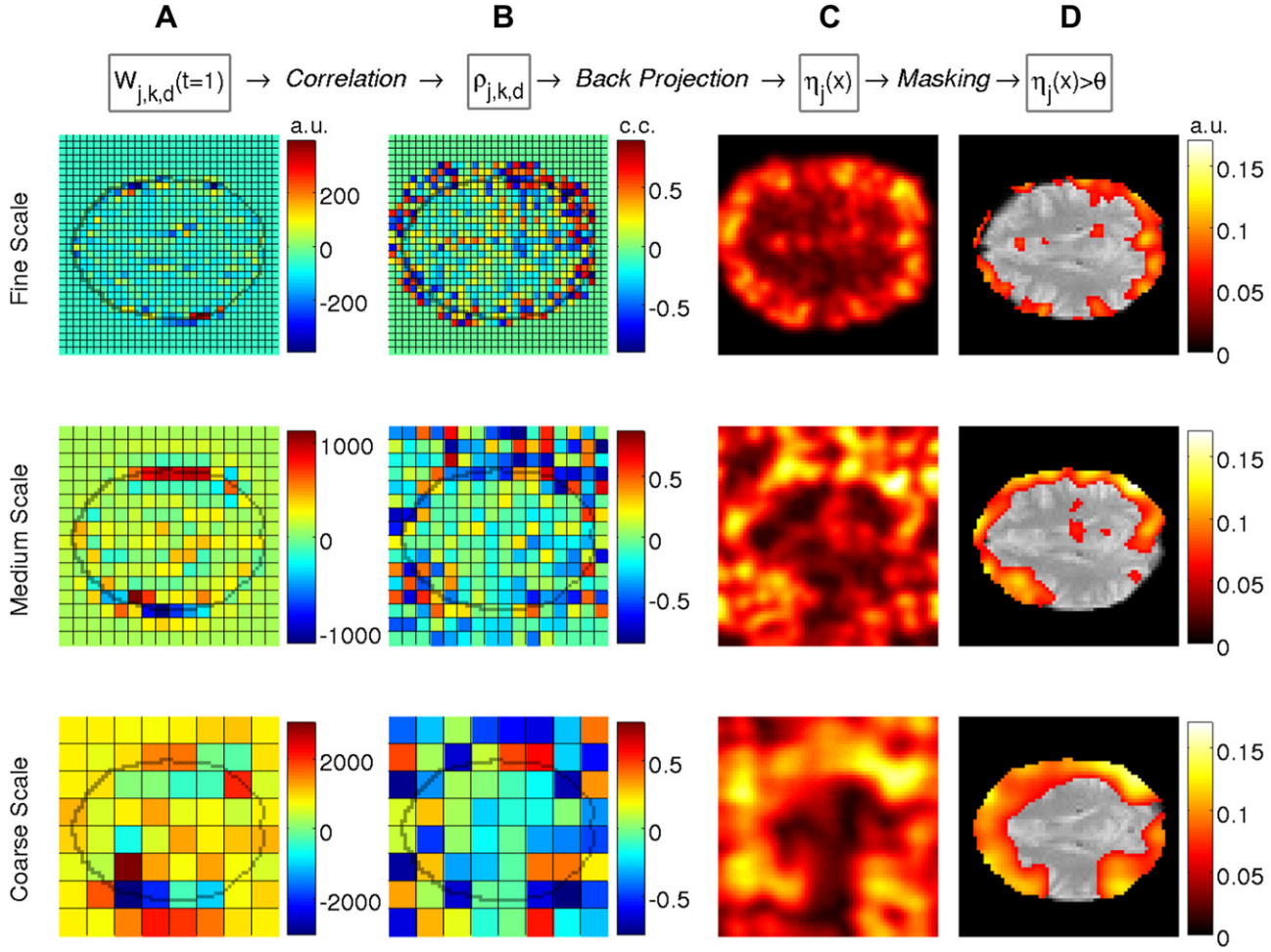

Fig. 2. Exemplified schematic representation of the proposed approach. The basis for the illustrative plots was 1) a time series of wavelet coefficients obtained by decomposing 3-dimensional BOLD images via the 3D DT-CWT and 2) the x-shift realignment parameters of that data set. A: Shown are the middle transversal planes of a 3D matrix $W_{j,k,d}$ of wavelet coefficients of a specific orientation d and of the indicated scale. This matrix belongs to the wavelet decomposition of the first BOLD image ($t = 1$) and the wavelet orientation corresponds to the orientation in Fig. 1A and 1B, fourth column from the left, second row from the top. The value of each wavelet coefficient is colour coded as indicated by colour bars. Furthermore, in order to facilitate a contrasting of the resolution to native space, the contour of the middle transversal plane of the raw BOLD image is plotted as an overlay on top of the coefficients matrices. The units of the wavelet coefficients are determined by the fMRI data. B: Middle transversal planes of the multiscale spatiotemporal correlation (MSC) map $\rho_{j,k,d}$ obtained by correlating each wavelet coefficient time series $W_{j,k,d}(1 \ldots N)$ with the realignment parameter x-shift. Correlation coefficient values are colour coded as indicated by colour bars. C,D: Middle transversal planes of the smoothed, scale-specific back projections $\eta_j(x)$, obtained from the MSC map $\rho_{j,k,d}$ by means of Equations (4) and (5). The units of the η-values are arbitrary and their values colour-coded as indicated by colour-bars. In D the back projection planes are masked for extra-cranial voxels and overlaid on the middle transversal plane of the decomposed raw BOLD image. Masking threshold is the 65th percentile of all η-values ($\theta = 0.06$).

illustration, cross-sections of in this way masked back projections are eventually overlaid on an anatomical template (Fig. 2D), e.g. the corresponding EPI cross-section.

2.7. Validation with a phantom data set

In order to validate the back projection approach, an analysis was conducted on an artificial phantom data set. This data set consisted of 600 volumes of size $64 \times 64 \times 32$ voxels, each initially consisting of uncorrelated and equally distributed white noise with zero mean and standard deviation 1. As reference signal we chose a simple boxcar function with 20 ON/OFF-oscillations consisting of 30 (arbitrary) time points each. As depicted in Fig. 3A, four ball-shaped voxel clusters are defined inside the volume. Next, the reference signal is added to the voxel time series inside a ball in such a way that the signal-to-noise ratio (SNR) of the resulting signal is 0.03, 0.06, 0.12 and 0.24 for each cluster respectively. This was achieved by scaling the boxcar signal such that $\mathrm{SNR} = \mathrm{mean}(S)/\mathrm{std}(N)$, where $\mathrm{std}(N)$ is the standard deviation of the noise. Each volume in the data set was wavelet decomposed by means of the 3D DT-CWT method and each hereby obtained wavelet coefficient time series correlated with the boxcar signal, yielding a MSC map which was subsequently back projected for each scale separately.

3. Results

3.1. Characterization and validation of methods

3.1.1. Precision of localization in spatial wavelet transformation

Before we present results of the MSC analysis, we want to exemplify some characteristics and implications of the wavelet decomposition of a BOLD image and its back projection into native space. In Fig. 2A the colour-coded 32×32, 16×16 and 8×8 matrices of wavelet coefficients depict the middle transversal planes of one decomposed BOLD image for a particular wavelet orientation and for each spatial scale. The magnitude of each coefficient reflects the amount of spatial variance in the corresponding location in the data along the specified orientation. The wavelet coefficients are not normalized; their magnitude is determined by the actual voxel intensities in the BOLD signal. Near locations of high variance in the data, in this case the transition from extra- to intra-cranial voxels, wavelet coefficients show the highest values and furthermore tend to oscillate. In Fig. 2A, this effect can be observed at the upper and lower edges of the brain slice in all three scales.

Another observation is that the range of the coefficient values substantially increases with scale. This derives from the fact that wavelets in coarser scales each detect variance in the data along a larger extent, thus capturing a larger amount of energy. This fact was considered in Eqs. (4) and (5) when defining a scale-specific weighting of correlation coefficients.

In Section 3.2 we will present the results of the MSC analysis using the realignment parameters as temporal predictor variables by examining the corresponding back projections in native space. However, beforehand it is of interest to consider the relationship between wavelet and native space with reference to the spatial distribution of correlation. A comparison of Fig. 2B and C shows that there is only rough correspondence of distributions of correlation in space between both domains. Single coefficients in wavelet space seem to be rather uninformative with respect to their precise location when directly mapped to native space (delineated in Fig. 2B by a grey line representing the brain surface). Therefore a direct mapping of the relative spatial location and extent of single coefficients into native space seems rather inappropriate. Rather, the conjoint inverse transform of the correlation coefficients is required to achieve a precise assessment of their spatial localization in native space.

3.1.2. Interpretation of back projections

In traditional imaging studies the significance of the obtained statistical parametric maps can be assessed by means of statistical inference, e.g. by applying the Gaussian field theory. This approach eventually yields well-localized and well-bounded voxel clusters associated with hemodynamic couplings with the temporal predictor variable. Our analysis, however, requires a somewhat specific approach in order to allow for an assessment of the obtained back projections of MSC maps.

While Eqn. (5) ensures that the back projection of one coefficient of same value yields in each scale an envelope with equal magnitude, the size (or spatial extent) of the envelope will increase with scale. Given the dyadic upsampling in the inverse transform, the radius of a smooth envelope will double with scale. This behaviour is not only expected but also convenient for our objective, since the spatial scale of a coefficient in wavelet space is reflected in the spatial extent of its reconstructed envelope. However, since the envelopes only slowly decay to zero, even areas in wavelet space with almost zero-valued coefficients will yield back projections where the corresponding areas show a certain level of η-values (cf. coefficient values in the center of the planes of Fig. 2B with corresponding back projections in Fig. 2C).

We therefore chose to apply the straightforward approach of thresholding the back projections at a certain η-level θ in order to discard low correlating and thus irrelevant areas and to emphasize 'hot spots' of high correlation. A pivotal point here is to choose the same threshold for all three scales, thus allowing for an explicit comparison of spatial extent increase between scales. The choice of the exact threshold is not critical and can be chosen such that it enhances the contrast of the inter-scale back projections. In Fig. 2D we chose the 65th percentile.

3.1.3. Noise sensitivity of the multiscale spatiotemporal correlation analysis

We sought to ascertain the performance of the MSC approach in identifying areas whose corresponding wavelet coefficient time series are correlated with some reference signal, and how this varies with the amount of background noise. We therefore performed our analysis on the artificial phantom data set. The scale-specific back projections thereby obtained are shown in Fig. 3B–D. They show the middle transversal planes of these back projections for the fine, medium and coarse scales, respectively.

The spatial extent of summed envelopes originating from high correlation coefficients in wavelet space increases with scale. Wavelet coefficients in the first scale only encode spatial variance on very small scales. Thus, only the contrast of successive activation and deactivation of the clusters' surface voxels with respect to the silent neighbouring outside voxels is detected in this scale, whereas the coarse scale encodes the activation of the entire voxel cluster.

Performance of the back projection in correctly detecting the spatial correlate of the signal increases with scale. In the back projection using only fine scale coefficients, the spatial correlate of the cluster with $\mathrm{SNR} = 0.24$ is clearly identifiable, while the ring of voxels corresponding to the sphere with $\mathrm{SNR} = 0.12$ is only barely discernible. In the back projection of the medium and coarse scales the sensitivity increases, allowing for detectability of the signal in the medium scale down to an SNR of 0.06 and likewise in the coarse scale down to an SNR of 0.03. In order to assert the quality of scale-specific reconstructions, a noise-free $32 \times 32 \times 32$ volume containing a sphere of voxels with the same arbitrary value was decomposed, correlated and back projected three times, once for

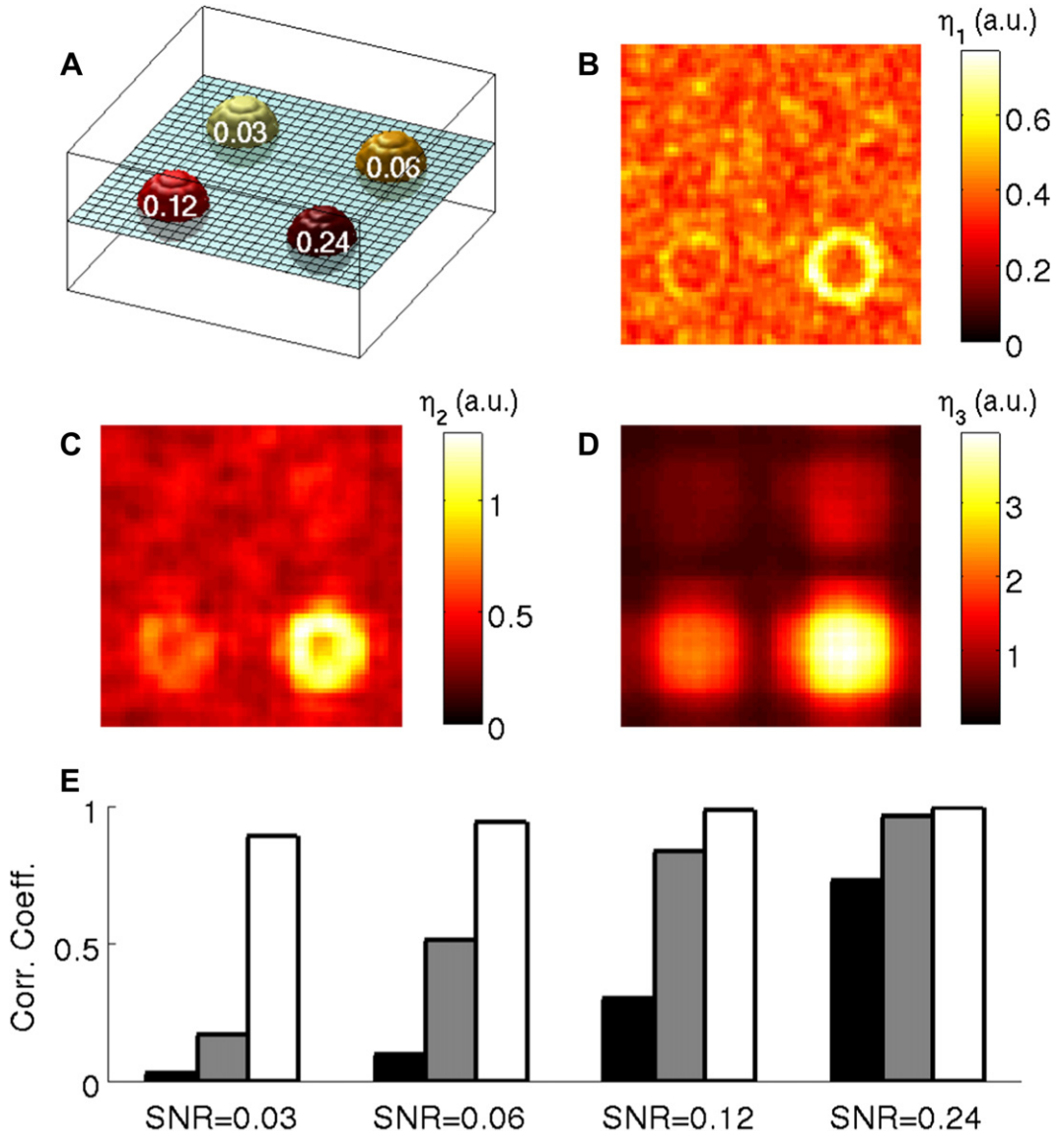

Fig. 3. Evaluation of sensitivity of the MSC analysis. A: Shown are four spheres contained in a $64 \times 64 \times 32$ volume. All voxels in this volume generate a time signal consisting of uncorrelated white noise. To the time series of voxels within a sphere the signal of an ON–OFF paradigm is added, in each sphere with a particular signal-to-noise ratio (SNR), as indicated in the plot. The blue plane indicates the location of the slices shown in plots B, C and D within the volume. B: The middle transversal plane of the reconstructed volume, using wavelet coefficients from the fine scale only. The units of the η-values are arbitrary. C, D: Analogous to plot B, for medium and large scales respectively. E: Three-dimensional correlation between noise-free and noisy back projections at SNRs of 0.03, 0.06, 0.12 and 0.24 at the fine (black), medium (gray) and coarse (white) scale.

each scale. Fig. 3E reports the correlation between the noise-free and the noisy back projections, for each scale and SNR. It reveals the increasing congruence with increasing scale as well as with increasing SNR. This speaks to the potential sensitivity of the approach to spatial variance that matches a particular level of the wavelet decomposition.

3.2. Multiscale spatiotemporal correlation of MR-realignment parameters

We subsequently applied our method to real EEG-fMRI data. Before testing the approach's capability to reveal relations between the alpha rhythm and fMRI activity at different spatial scales, we chose to investigate its susceptibility to movement-related residual spatial variance in fMRI data and the effect of an additional movement correction.

MSC analysis with the six realignment parameters was performed on fMRI data preprocessed under two conditions, namely with and without correction of residual movement artefacts. In Fig. 4 we present results of subject d who exhibits strongest effects due to high residual movement-related variance. Before additional motion correlation (Fig. 4A), a striking feature among all maps is that, across all parameters and scales, the highest magnitudes are localized solely on the edges (and hence on the surface since these are transversal cross-sections) of the brain. Moreover, a high similarity between the reconstructions of certain parameters and scales is evident in terms of spatial structure and magnitude.

Thus, results indicate a high susceptibility of the approach to brain movement, in terms that a spatial displacement of the brain during recording will have a large effect on the wavelet coefficient time series particularly at the outer and inner surfaces of the brain. Fig. 4B shows the results of the MSC analysis after the removal of residual movement-related variance from the fMRI data. After correction, MSC maps of realignment parameters *y*, *z*, pitch and roll do not contain any significant correlation coefficients at all, thus no

back projection is obtained. MSC maps of parameters *x* and yaw still show some residual correlation, however, the η-values of their back projections decrease by roughly one order of magnitude.

3.3. Multiscale spatiotemporal correlation of EEG posterior alpha rhythm

We performed analysis of EEG-fMRI data by correlating EEG signatures with the fMRI wavelet coefficient time courses. The signature chosen was the classical posterior alpha rhythm, which was identified via ICA as done in Becker et al. (2008). There are several obvious advantages for choosing this component. First, the posterior alpha rhythm has very pronounced amplitudes and is clearly identifiable in most healthy subjects. Furthermore, the posterior alpha rhythm component as extracted by ICA is usually less contaminated by signals of non-neuronal origin such as eye movements or residual cardiac and respiratory artefacts.

Analogous to the previous analysis, we initially sought to verify that the removal of residual movement-related variance improves the MSC analysis when using a physiologically relevant signal as a temporal predictor variable. Therefore, via MSC analysis the EEG alpha IC-component power time series were used to obtain three back projections, one for each spatial scale. This analysis was done twice, both on the realigned and on the additionally motion corrected fMRI data. In Fig. 5A we present the results of subject a for the analysis with the realigned fMRI data. In all three back projections both the location of the highest η-values on the surface of the brain and their value range are consistent with the results from the MSC analysis using the realignment parameters (Fig. 4A). After an additionally removing residual movement-related variance (Fig. 5B, top row), peak η-values decreased by a factor of roughly five and the ring-shaped distributions had been replaced by distributions with emphasis on occipital areas with a great overlap with visual cortical areas. Note that colour-coding and masking threshold are different between the two sets of back projections, but are equal among the three spatial scales in each analysis. The remaining rows in Fig. 5B show the results of subjects b, c and d after movement correction of fMRI data. As in subject a, in all three subjects the spatial distribution of high η-values shows an emphasis on occipital areas with a clear overlap with visual cortical areas.

In all four subjects the obtained η-values vary for the three scales in terms that both the mean magnitude and the spatial extent seem to increase with scale. While the latter behaviour is expected due to the increase of envelopes with scale, the former may be due to the differential degree of the effect of white noise. However, it is also consistent with the hypothesis that alpha (slow rhythms) mediates longer range coupling in the brain. Future analyses comprising EEG beta and gamma bands will elucidate whether the found dependency on scale is a reflection of noise or a coupling of scales as hypothesized in the introduction.

4. Discussion

Empirical evidence that higher frequency rhythms emerge locally whereas lower frequencies involve larger brain regions supports the hypothesis that rhythms serve as integrators across distributed neuronal populations of varying spatial extent (Draguhn et al., 1998; von Stein and Sarnthein, 2000; von Stein et al., 2000; Csicsvari et al., 2000; Kopell et al., 2000; Engel et al., 2001; Contreras and Llinás, 2001; Varela et al., 2001; Buzsáki, 2002; Sirota et al., 2003; Steriade and Timofeev, 2003). Simultaneous EEG and fMRI acquisitions offer a promising basis for testing the above theory because brain activity can be assessed in the temporal and spatial domain from highly resolved scales through to its global extent, i.e. the entire cortex. Although EEG and the BOLD signal recorded in fMRI reflect different processes of neural activity, they are tightly coupled (Logothetis et al., 2001) and prior research has established that variation in the spectral power of EEG rhythms is accompanied by changes in metabolism or blood flow. Traditional fMRI-EEG analyses first convolve the envelope of ongoing amplitude fluctuations with the hemodynamic response function (HRF), which takes into account the delay of the vascular response. By applying statistical parametric mapping, several studies have shown correlations between the BOLD signal and spontaneous power fluctuations of diverse brain rhythms.

However, these studies analyze the temporal dynamics of EEG in the frequency domain, while they look at the spatial domain of the BOLD signal in a voxel-wise manner. Whilst offering exciting insights, this approach is not able to establish a mapping between temporal frequencies and their typical spatial scales. In this study we hence demonstrate proof of concept for a novel approach for the analysis of simultaneous EEG-fMRI data that aims at providing evidence for a systematic link between spatial and temporal scales of brain dynamics.

We have demonstrated that the three-dimensional wavelet transform, and in particular the 3D DT-CWT, is suited for the analysis of the spatial spectrum of BOLD images. After decomposing each volume of an fMRI time series, the resulting temporal dynamics of the local spatial variance can be correlated with the temporal dynamics of another instantaneously occurring process such as the power of a particular frequency band of simultaneously acquired EEG data. In this way a localized multiscale representation of the strength of correlation is obtained. Finally, by means of an inverse wavelet transform, this representation is projected back into native space, thus revealing localized, band-specific and scale-specific magnitude maps of multiscale spatio-temporal correlation.

Our approach is an example of a scale-space search, which has been introduced in the context of functional neuroimaging in the 90s (Worsley et al., 1992; Friston et al., 1994; Poline et al., 1997; Kiebel et al., 1999]. The idea here was to repeat the statistical analysis (using Statistical Parametric Mapping) on data that were successively smoothed in space. The ensuing SPMs were then endowed with an extra dimension (smoothness), such that significant correlations appeared as blobs in anatomical and scale-space. It was proposed to use random field theory to correct for the implicit multiple comparisons induced by the scale-space search. We envisage that similar approaches will be required to interpret our correlation maps. However, one advantage of our discrete wavelet transform is that multiple comparisons do not pose a major problem, because we only have to worry about a limited number of spatial scales.

4.1. Motivation for the back-projection approach

Having obtained a particular MSC map, one simple and straightforward analysis approach would be to directly map the contained coefficients to native space. Direction-specific MSC matrices of one scale can be summed up and subsequently mapped to native space via dyadic upsampling. However, the overlays of the brain slice edges on top of the MSC map cross-sections in Fig. 2B indicate that particularly in coarser scales the spatial distribution of coefficients clearly extends to regions outside the brain, rendering such a direct mapping unsuitable.

These shortcomings motivate a novel approach based upon back projection of the wavelet coefficients. This provides a way of mapping the MSC matrices back to native space, making use of the possibility given by the DT-CWT to reconstruct non-oscillatory envelopes. This approach offers several advantages. Firstly, the dyadic upsampling during back projection yields a representation

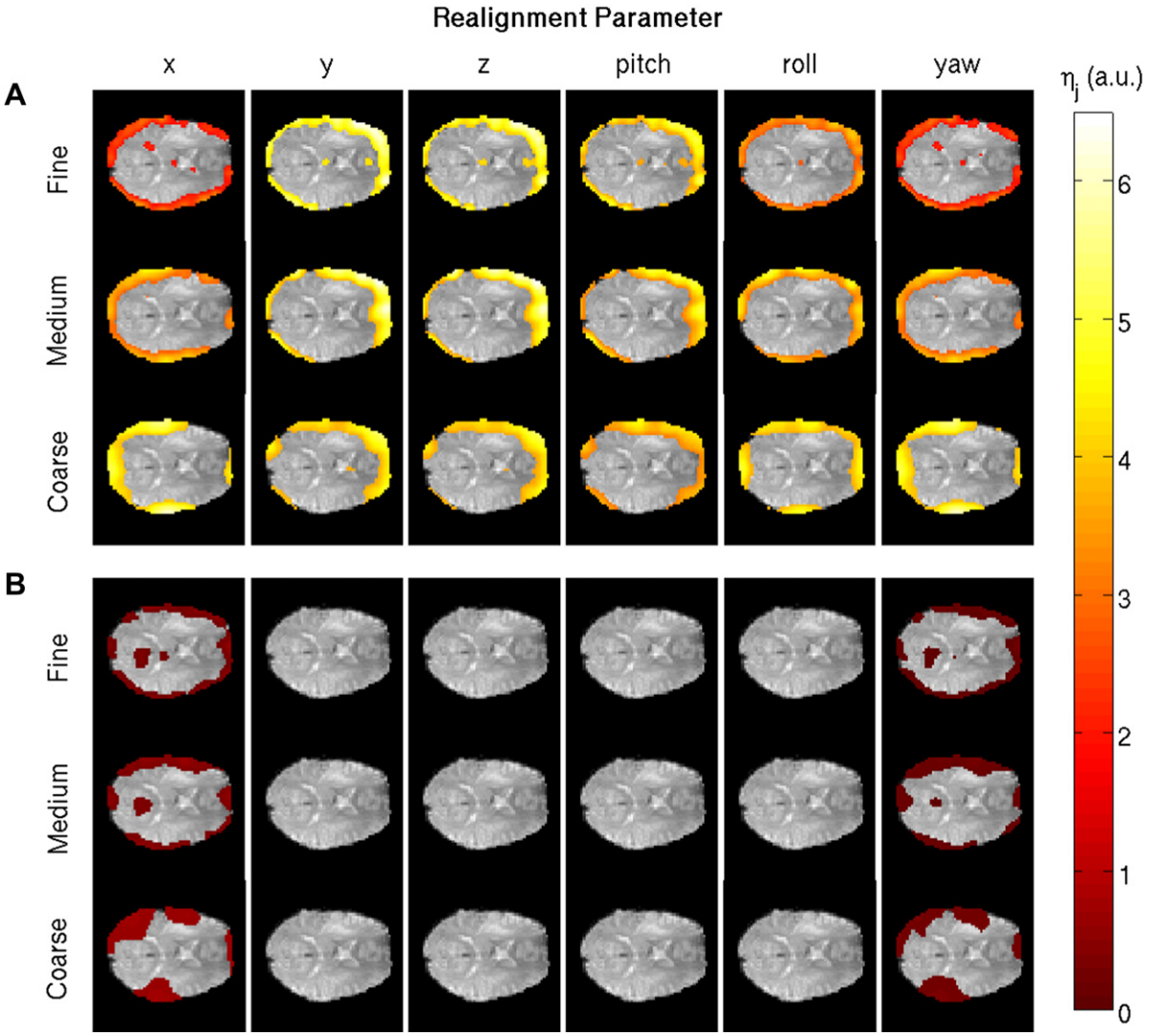

Fig. 4. Multiscale spatiotemporal correlation (MSC) between realignment parameters and fMRI-signal at three spatial scales. Scale-specific back projections of MSC maps were obtained from the six realignment parameters and performed on realigned fMRI data (A) and after additional motion correction (B). In each slice, the middle transversal planes of the masked and smoothed back projections of subject d are shown, superimposed on the corresponding middle transversal plane of the raw BOLD image. Here, for each slice anatomical anterior-posterior corresponds to left-right, and anatomical left-right corresponds to top-down. Note that the masking threshold (75th percentile) was determined for each slice separately. The colour-coding is equal for all plots, η-value units are arbitrary.

of the MSC map at the same resolution as the original data, making a direct mapping expedient. Furthermore, the envelope magnitudes in the back projections now allow the qualitative comparison of the total amount of correlation between scales. However, due to the non-linear property of the back projection approach (see equation (4)), there is no direct relationship between the correlation coefficients in wavelet space and the back projected η-values in native space.

4.2. Evaluation of the MSC analysis by phantom data

Before applying the back projection procedure on multiscale spatiotemporal correlation maps of the EEG-fMRI data, we tested the theoretical ability of our approach to reconstruct dynamics of spatial variance in the presence of noise. Assume a back projected MSC map, generated from a data set in which the activity of a certain cluster of voxels is correlated with the reference signal. In this context two particularly important questions arise: i) What are the differences between spatial scale-specific back projections of that cluster, and ii) how does the MSC analysis depend on the SNR in the data?

In order to address these issues, we tested performance of our algorithm on an artificial phantom data set. The results from this simulation study (Fig. 3) provide a means of approaching the above questions. As one would expect, fine scale coefficients exclusively detect the signal contrast at the borders of the activated area, in this case reconstructing an empty sphere. Coarse scale coefficients, in contrast, are able to detect the activation of the area as a whole. Of course the proportionality of each scale in the back projection strongly depends on the geometric structure of the activated area. The shape of the area chosen in the simulated data represents an extremely simple geometric form with a smooth surface. In fact, of all possible geometric shapes, a sphere entails the least variance at fine spatial scales. This simplification may be inappropriate considering the diversity of conceivable geometric patterns functional brain areas may exhibit. Given the complex architecture of the numerous gyri and sulci, one can expect that a cluster of voxels forming a functionally coherent brain area will have a rather

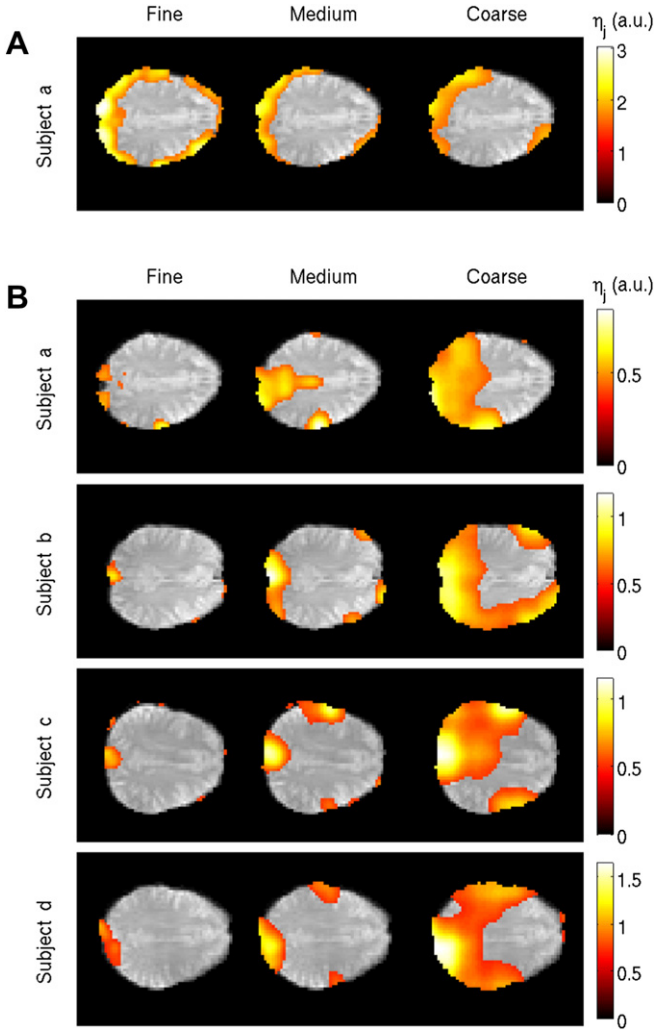

Fig. 5. Multiscale spatiotemporal correlation (MSC) between EEG alpha rhythm power and fMRI-signal at different spatial scales. Scale-specific back projections of MSC maps were obtained from posterior EEG alpha rhythm (identified via ICA) and performed on realigned (A; only subject a) and additionally motion corrected (B; all four subjects) fMRI data. Shown in each slice are the middle transversal planes of the masked and smoothed back projections, superimposed on the corresponding middle transversal planes of the raw BOLD images. Colour-coding and masking threshold (75th percentile) are equal for the three spatial scales of one subject, η-value units are arbitrary. We find areas with highest η-values located in neuroanatomically plausible visual areas.

irregular shape, thus increasing the occurrence and amount of spatial variance at fine scales. This, however, would not be expected to completely obscure possible relations between brain rhythms and the spatial extents of neuronal activity for given brain regions.

Regarding the second question, the analysis shows that the MSC sensitivity in terms of SNR increases with scale. This may arise from the fact that we used white Gaussian noise in the simulations. Since at the end of each iteration of the deconstructing algorithm the data is dyadically downsampled, the amount of noise is effectively reduced by a factor of $\sqrt{2^3}$. As a consequence correlations are expected to be higher at coarser scales, thus enhancing the sensitivity as well as increasing envelope magnitudes. The use of $1/f$ noise – more precisely reflecting the known physiological features in BOLD data – might be instructive in future simulations.

Given that typical SNR levels reported in fMRI experiments lie roughly between 2% and 8%, one has to be careful when interpreting results in the fine and medium scales of EEG/fMRI data. Here, a scale-specific thresholding (depending on observed distribution of p-values) may reduce this bias. One approach to this problem might be to normalize the correlations to those obtained from "wavestrapped" surrogate data (Breakspear et al., 2004).

4.3. Back projection

Movements of the brain are reflected mainly by an increase of variance at the brain-tissue borders. Although the images were realigned before decomposition using the estimated RBT parameters, residual motion-based changes of spatial variance over time yielded back projections that clearly indicate high correlations at the brain's tissue borders (Fig. 4). Evidently, our method is able to reveal residual movement artefacts in the BOLD signal in the back projections. It should be noted, that such edge patterns can also typically be observed in voxel-wise regressions which is why the movement parameters are usually modeled as nuisance regressors in typical GLM.

In order to avoid including movement related variance of fMRI data in our MSC maps our efforts were twofold: 1) removal of movement related variance from fMRI data and 2) removal of movement related variance from EEG data. The latter point was achieved by employing temporal ICA on the EEG data and then manually selecting the independent component best representing the posterior alpha rhythm. Since this band is so pronounced in the posterior part of the brain, an identification of such a component based on spectral characteristics and topography is possible in most cases. For the removal of residual movement related variance in the fMRI data we chose to estimate that variance using the realignment parameters in a linear model and subtract the projection of this estimate on the data from the raw data.

MSC back projections of all four subjects yielded biologically plausible distributions located within the visual cortex. Given that the reference signal here is the posterior alpha rhythm, the evident occipital emphasis of reconstructed correlation is considered as an evidence for the validity of our approach. The localization of high η-magnitudes is in accordance with findings from previous studies using traditional analysis methods, e.g. Moosmann et al. (2003).

This study was conceptualized to provide proof of concept of the proposed method. Hence looking into other EEG frequency bands – and into trends concerning their correlation with spatial scales will be subject to future analyses. In the case of the presently employed posterior alpha rhythm, the mean intensity of η-values increased with scale in the four data sets (Fig. 5). As stated above, this effect might be attributed to the fact that SNR increases for coarser scales. For comparison of the amount of correlation across scales a normalizing factor accounting for this bias needs to be employed. A possible extension and improvement may be based on Bayesian wavelet approaches such as demonstrated in Turkheimer et al. (2006). There, magnitudes from coarser scales were used as priors for finer ones, thus reducing the bias introduced by scale specific noise.

Future comparisons of the findings related to the alpha rhythm with that of other rhythms may reveal interesting features of the time-space relationship of brain activity. Candidate rhythms are those of the classical EEG frequency bands: gamma (>30 Hz), beta (13–29 Hz), theta (5–11 Hz) and delta (1–4 Hz). While there is wide agreement that EEG reflects delta to beta band activity, an ongoing debate exists to which extent true gamma activity rather than microsaccade artefacts are assessed by EEG (Yuval-Greenberg et al., 2008). It has been noted, however, that there exist a number of studies, where an artificial microsaccade-related origin of gamma band activity in the EEG can be ruled out (Schwartzman and Kranczioch, 2010). With respect to the possibility of assessing the gamma rhythm in resting state rather than in task data, this has been achieved before in an MEG study reporting a systematic relation between gamma power variations and the ongoing alpha

rhythm (Osipova et al., 2008) and in an EEG study reporting a systematic relation to ongoing theta band power as well as to subsequently tested short-term memory capacity EEG (Kaminski et al.). By means of simultaneous EEG-fMRI meaningful relations between the time series of gamma band activity and hemodynamics have been identified for an auditory choice reaction task (Mulert et al., 2010) and for rest conditions (Mantini et al., 2007; Ritter et al., 2008a,b).

Hence several conditions would be suitable for the investigation of spatiotemporal nesting by the proposed approach based on simultaneously acquired EEG-fMRI data. One should be aware, however, that the sites of spatiotemporal nesting might vary for different brain states or task conditions. Consequently appropriate analysis tools need to be employed being able to account for spatial non-stationarity.

5. Conclusion

We developed a novel technique for analyzing the multiscale spatiotemporal correlation structure in resting state EEG-fMRI data. We have presented an approach that performs a back projection of this correlation structure, which is represented in wavelet space, back into the native domain. It provides a straightforward way of localizing the strength of multiscale spatiotemporal correlation within the brain, depending on spatial scale and band frequency. By means of analyzing a simulated phantom data set, we identified certain scale-specific characteristics of the back projection and furthermore assessed its sensitivity to noise. On the whole, these preliminary findings provide a starting point for further exploiting the full potential that this analysis approach may offer.

Several previous studies have used spatial wavelets for the analysis of fMRI data. However, to our knowledge, the present study is the first to analyze the multiscale spatiotemporal correlation structure of simultaneously acquired EEG/fMRI data. By means of the present empirical findings and derived theoretical considerations, we identified certain pitfalls, which arose in the implementation of the presented approach. These issues have to be solved in order to fully unlock the potential of this method for investigating the relationship between oscillatory rhythms in the EEG and the spatial variance of the BOLD signal. We believe that, based on our findings and by including the proposed enhancements, this approach can serve as a suitable tool for future research of the deep spatiotemporal structure of cortical processes.

Acknowledgments

This work was supported by the German Federal Ministry of Education and Research BMBF (Bernstein Center for Computational Neuroscience, Bernstein Focus State Dependencies of Learning), the German Research Foundation DFG (Berlin School of Mind and Brain), the Max Planck Society (Max Planck Institute for Human Cognitive and Brain Sciences, Department of Neurology) and the Robert Bosch Foundation.

References

Abdelnour, A., Selesnick, I., 2001. Design of 2-band orthogonal near-symmetric CQF. In: ICASSP Conference, vol. 6, pp. 3693–3696.
Andersson, J.L., Hutton, C., Ashburner, J., Turner, R., Friston, K., 2001. Modeling geometric deformations in EPI time series. NeuroImage 13, 903–919.
Bandettini, P., Jesmanowicz, A., Wong, E., Hyde, J., 1993. Processing strategies for time-course data sets in functional MRI of the human brain. Magnet. Resonan. Med. 30, 161–173.
Becker, R., Ritter, P., Villringer, A., 2008. Influence of ongoing alpha rhythm on the visual evoked potential. NeuroImage 39, 707–716.
Berger, H., 1929. Über das Elektroenkephalogramm des Menschen. Arch.-Psychiat.Nervenkr 87, 527–570.
Brammer, M.J., 1998. Multidimensional wavelet analysis of functional magnetic resonance images. Hum. Brain Mapp. 15, 763–770.
Breakspear, M., Brammer, M., Dass, P., Bullmore, E., Williams, L.M., 2004. Spatiotemporal wavelet resampling for functional neuroimaging data. Hum. Brain Mapp. 23, 1–25.
Breakspear, M., Bullmore, E.T., Aquino, K., Das, P., Williams, L.M., 2006. The multiscale character of evoked cortical activity. NeuroImage 30, 1230–1242.
Bullmore, E.T., Long, C., Suckling, J., Fadili, J., Calvert, G., Zelaya, F., Carpenter, T., Brammer, M.J., 2001. Colored noise and computational inference in neurophysiological time series analysis: resampling methods in time and wavelet domains. Hum. Brain Mapp. 12, 61–78.
Bushara, K.O., Hanakawa, T., Immisch, I., Toma, K., Kansaku, K., Hallett, M., 2003. Neural correlates of cross-modal binding. Nat. Neurosci. 6, 190–195.
Buzsáki, G., 2002. Theta oscillations in the hippocampus. Neuron 33, 325–340.
Buzsáki, G., 2006. Rhythms of the Brain. Oxford University Press, USA.
Buzsáki, G., Buhl, D.L., Harris, K.D., Csicsvari, J., Czeh, B., Morozov, A., 2003. Hippocampal network patterns of activity in the mouse. Neuroscience 116, 201–211.
Contreras, D., Llinas, R., 2001. Voltage-sensitive dye imaging of neocortical spatiotemporal dynamics to afferent activation frequency. J. Neurosci. 21, 9403–9413.
Csicsvari, J., Hirase, H., Mamiya, A., Buzsáki, G., 2000. Ensemble patterns of hippocampal CA3-CA1 neurons during sharp wave-associated population events. Neuron 28, 585–594.
Daubechies, I., 1988. Orthonormal bases of compactly supported wavelets. Commun. Pure Appl. Math. 41, 909–996.
Daubechies, I., 1990. The wavelet transform, time-frequency localisation and signal analysis. IEEE Trans. Inform. Theory 36, 961–1005.
Daubechies, I., 1993. Orthonormal bases of compactly supported wavelets. II. Variations on a theme. SIAM J. Math. Anal. 24, 499–519.
Daubechies, I., 1992. Ten lectures on wavelets, volume 61 of CBMS-NSF Regional Conference Series in Applied Mathematics. Society for Industrial and Applied Mathematics (SIAM), Philadelphia, PA.
Debener, S., Mullinger, K., Niazy, R., Bowtell, R., 2008. Properties of the ballistocardiogram artefact as revealed by EEG recordings at 1.5, 3 and 7 T static magnetic field strength. Int. J. Psychophysiol. 67, 189–199.
de Munck, J.C., Goncalves, S.I., Huijboom, L., Kuijer, J.P., Pouwels, P.J., Heethaar, R.M., Lopes da Silva, F.H., 2007. The hemodynamic response of the alpha rhythm: an EEG/fMRI study. NeuroImage 35 (3), 1142–1151.
Difrancesco, M.W., Holland, S.K., Szaflarski, J.P., 2008. Simultaneous EEG/functional magnetic resonance imaging at 4 Tesla: correlates of brain activity to spontaneous alpha rhythm during relaxation. J. Clin. Neurophysiol. 25, 255–264.
Dinov, I.D., Boscardin, J.W., Mega, M.S., Sowell, E.L., Toga, A.W., 2005. A waveletbased statistical analysis of fMRI data: I. motivation and data distribution modeling. Neuroinformatics 3, 319–342.
Draguhn, A., Traub, R.D., Schmitz, D., Jefferys, J.G.R., 1998. Electrical coupling underlies high-frequency oscillations in the hippocampus in vitro. Nature 394, 189–192.
Engel, A.K., Fries, P., Singer, W., 2001. Dynamic predictions: oscillations and synchrony in top-down processing. Nat. Rev. Neurosci. 2, 704–716.
Fadili, J., Bullmore, E., 2002. Spatiotemporal wavelet analysis for functional MRI. NeuroImage 15, 217–232.
Feige, B., Scheffler, K., Esposito, F., Di Salle, F., Hennig, J., Seifritz, E., 2005. Cortical and subcortical correlates of electroencephalographic alpha rhythm modulation. J. Neurophysiol. 93, 2864–2872.
Friston, K.J., Worsley, K.J., Frackowiak, R.S.J., Mazziotta, J.C., Evans, A.C., 1994. Assessing the significance of focal activations using their spatial extent. Hum. Brain Mapp. 1, 210–220.
Friston, K.J., Frith, C.D., Turner, R., Frackowiak, R.S.J., 1995a. Characterizing evoked hemodynamics with fMRI. Hum. Brain Mapp. 2, 157–165.
Friston, K.J., Ashburner, J., Frith, C.D., Poline, J.-B., Heather, J.D., Frackowiak, R.S.J., 1995b. Spatial registration and normalization of images. Hum. Brain Mapp. 2, 165–189.
Friston, K.J., Williams, S., Howard, R., Frackowiak, R.S., Turner, R., 1996. Movement-related effects in fMRI time-series. Magn. Reson. Med. 35, 346–355.
Goldman, R.I., Stern, J.M., Engel, J., Cohen, M.S., 2002. Simultaneous EEG and fMRI of the alpha rhythm. Neuroreport 13, 2487–2492.
Goncalves, S.I., de Munck, J.C., Pouwels, P.J., Schoonhoven, R., Kuijer, J.P., Maurits, N.M., Hoogduin, J.M., Van Someren, E.J., Heethaar, R.M., Lopes da Silva, F.H., 2005. Correlating the alpha rhythm to BOLD using simultaneous EEG/fMRI: Inter-subject variability. NeuroImage 30, 203–213.
Hilton, M., Hattery, D., Jawerth, G., Eden, B., 1996. Wavelet denoising of functional MRI data. In: Aldroubi, A., Unser, M. (Eds.), Wavelets in Biology and Medicine. CRC Press, pp. 93–114.
Jensen, O., Colgin, L.L., 2007. Cross frequency coupling between neuronal oscillations. Trends Cogn. Sci. 11, 267–269.
Kaminski, J., Brzezicka, A., Wrobel, A., Short-term memory capacity (7+/−2) predicted by theta to gamma cycle length ratio. Neurobiol. Learn Mem.
Kiebel, S.J., J-Poline, B., Friston, K.J., Holmes, A.P., Worsley, K.J., December 1999. Robust smoothness estimation in statistical parametric maps using standardized residuals from the general linear model. NeuroImage 10 (6), 756–766.
Kingsbury, N., 1998. The dual-tree complex wavelet transform: a new efficient tool for image restoration and enhancement. In: The 9th European Signal Processing Conference.
Kingsbury, N., 1999. Image processing with complex wavelets. Phil. Trans. R. Soc. London. A: Math., Phys. Eng. Sci. 357, 2543–2560.

Kingsbury, N., 2001. Complex wavelets for shift invariant analysis and filtering of signals. Appl. Comput. Harmonic Anal. 10, 234–253.
Koch, S.P., Werner, P., Steinbrink, J., Fries, P., Obrig, H., 2009. Stimulus-induced and state-dependent sustained gamma activity is tightly coupled to the hemodynamic response in humans. J. Neurosci. 29, 13962–13970.
Kopell, N., Ermentrout, G.B., Whittington, M.A., Traub, R.D., 2000. Gamma rhythms and beta rhythms have different synchronization properties. Proc. Natl. Acad. Sci. U..S…..A 97, 1867–1872.
Laufs, H., Kleinschmidt, A., Beyerle, A., Eger, E., Salek-Haddadi, A., Preibisch, C., Krakow, K., 2003. EEG-correlated fMRI of human alpha activity. NeuroImage 19, 1463–1476.
Logothetis, N.K., Pauls, J., Augath, M., Trinath, T., Oeltermann, A., 2001. Neurophysiological investigation of the basis of the fMRI signal. Nature 412, 150–157.
Long, C., Brown, E.N., Manoach, D., Solo, V., 2004. Spatiotemporal wavelet analysis for functional mri. NeuroImage 23, 500–516.
Mallat, S.G., 1989. A theory for multiresolution signal decomposition: the wavelet representation. IEEE Trans. Pattern Anal. Mach. Intell. 11, 674–693.
Mantini, D., Perrucci, M.G., Del Gratta, C., Romani, G.L., Corbetta, M., 2007. Electrophysiological signatures of resting state networks in the human brain. Proc. Natl. Acad. Sci. U.S.A. 104, 13170–13175.
Moosmann, M., Ritter, P., Krastel, I., Brink, A., Thees, S., Blankenburg, F., Taskin, B., Obrig, H., Villringer, A., 2003. Correlates of alpha rhythm in functional magnetic resonance imaging and near infrared spectroscopy. NeuroImage 20, 145–158.
Mulert, C., Leicht, G., Hepp, P., Kirsch, V., Karch, S., Pogarell, O., Reiser, M., Hegerl, U., Jager, L., Moller, H.J., McCarley, R.W., 2010. Single-trial coupling of the gamma-band response and the corresponding BOLD signal. NeuroImage 49, 2238–2247.
Niessing, J., Ebisch, B., Schmidt, K.E., Niessing, M., Singer, W., Galuske, R.A., 2005. Hemodynamic signals correlate tightly with synchronized gamma oscillations. Science (New York, N.Y.) 309, 948–951.
Osipova, D., Hermes, D., Jensen, O., 2008. Gamma power is phase-locked to posterior alpha activity. PLoS ONE 3, e3990.
Poline, J.B., Worsley, K.J., Evans, A.C., Friston, K.J., 1997. Combining spatial extent and peak intensity to test for activations in functional imaging. NeuroImage 5, 83–96.
Ritter, P., Becker, R., Graefe, C., Villringer, A., 2007. Evaluating gradient artifact correction of EEG data acquired simultaneously with fMRI. Magn. Reson. Imaging 25, 923–932.
Ritter, P., Moosmann, M., Villringer, A., 2009. Rolandic alpha and beta EEG rhythms' strengths are inversely related to fMRI-BOLD signal in primary somatosensory and motor cortex. Hum. Brain Mapp. 30, 1168–1187.
Ritter, P., Villringer, A., 2006. Simultaneous EEG-fMRI. Neurosci. Biobehav. Rev. 30, 823–838.
Ritter, P., Greicius, M., Becker, R., Villringer, A., 2008a. Relation between spatially and spectrally confined EEG rhythms and fMRI resting state networks. Abstract contribution at the 14th Human Brain Mapping conference, Melbourne.
Ritter, P., Freyer, F., Curio, G., Villringer, A., 2008b. High-frequency (600 Hz) population spikes in human EEG delineate thalamic and cortical fMRI activation sites. NeuroImage 42, 483–490.
Ritter, P., Becker, R., Freyer, F., Villringer, A., 2010. EEG quality: the image acquisition artefact. In: Mulert, C., Lemieux, L. (Eds.), EEG – fMRI physiological basis, technique, and applications. Springer, Berlin Heidelberg, pp. 153–171.
Ruttimann, U.E., Ramsey, N.F., Hommer, D.W., Thevenaz, P., Lee, C., Unser, M., 1995. Analysis of functional magnetic resonance images by wavelet decomposition. In: ICIP '95: Proceedings of the 1995 International Conference on Image Processing, vol. 1. IEEE Computer Society, Washington, DC, USA, p. 633.
Schwartzman, D., Kranczioch, C., 2010. In the blink of an eye. The contribution of microsaccadic activity to the induced gamma band response. Int. J. Psychophysiol..
Selesnick, I.W., Li, K.Y., 2003. Video denoising using 2D and 3D dual-tree complex wavelet transforms. In: Unser, M.A., Aldroubi, A., Laine, A.F. (Eds.), Society of Photo-Optical Instrumentation Engineers (SPIE) Conference Series, volume 5207 of Presented at the Society of Photo-Optical Instrumentation Engineers (SPIE) Conference, pp. 607–618. doi: 10.1117/12.504896.
Selesnick, -I.W., Baraniuk, R.G., Kingsbury, N.C., 2005. The dual-tree complex wavelet transform. Signal Processing Magazine. IEEE 22 (6), 123–151.
Sirota, A., Csicsvari, J., Buhl, D., Buzsaki, G., 2003. Communication between neocortex and hippocampus during sleep in rodents. Proc. Natl. Acad. Sci. U.S.A. 100, 2065–2069.
Steriade, M., Timofeev, I., 2003. Neuronal plasticity in thalamocortical networks during sleep and waking oscillations. Neuron 37, 563–576.
Turkheimer, F.E., Aston, J.A., Asselin, M.C., Hinz, R., 2006. Multi-resolution Bayesian regression in PET dynamic studies using wavelets. NeuroImage 32, 111–121.
Van De Ville, D., Blu, T., Unser, M., 2004. Integrated wavelet processing and spatial statistical testing of fMRI data. NeuroImage 23, 1472–1485.
Varela, F., Lachaux, J.P., Rodriguez, E., Martinerie, J., 2001. The brainweb: phase synchronization and large-scale integration. Nat. Rev. Neurosci. 2, 229–239.
von Stein, A., Sarnthein, J., 2000. Different frequencies for different scales of cortical integration: from local gamma to long range alpha/theta synchronization. Int. J. Psychophysiol. 38, 301–313.
von Stein, A., Chiang, C., König, P., 2000. Top-down processing mediated by interareal synchronization. Proc. Natl. Acad. Sci. U.S.A. 97, 14748–14753.
Weeks, M., Bayoumi, M., 2003. Discrete wavelet transform: architectures, design and performance issues. VLSI Signal Process. 35, 155–178.
Worsley, K.J., Evans, A.C., Marrett, S., Neelin, P., 1992 Nov. A three-dimensional statistical analysis for CBF activation studies in human brain. J. Cereb. Blood Flow Metab. 12 (6), 900–918.
Yuval-Greenberg, S., Tomer, O., Keren, A.S., Nelken, I., Deouell, L.Y., 2008. Transient induced gamma-band response in EEG as a manifestation of miniature saccades. Neuron 58, 429–441.